Solvent-Free Preparation of Nanosized Sulfated Zirconia with Brønsted Acidic Sites from a Simple Calcination

Yinyong Sun,[†] Shengqian Ma,[†] Yunchen Du,[†] Lina Yuan,[†] Shichao Wang,[†] Jun Yang,[‡] Feng Deng,[‡] and Feng-Shou Xiao*[,†]

College of Chemistry & State Key Laboratory of Inorganic Synthesis and Preparative Chemistry, Jilin University, Changchun 130023, China, and State Key Laboratory of Magnetic Resonance and Atomic and Molecular Physics, Wuhan Institute of Physics and Mathematics, Chinese Academy of Sciences, Wuhan 430071, China

Received: August 13, 2004; In Final Form: November 26, 2004

Nanosized sulfated zirconia with Brønsted acidic sites has been prepared by a simple calcination in the absence of any solvent. XRD patterns reveal that the sulfated zirconia mainly consists of tetragonal crystalline zirconia with average size of about 7 nm, which is further confirmed by TEM images. N_2 adsorption data show that the nanosized sulfated zirconia has high surface area (165−193 m^2/g) and exhibits uniform pore distribution aggregated by zirconia nanoparticles. IR spectra of samples show that the sulfur species in the nanosized sulfated zirconia is a little different from that in conventional sulfated zirconia. Furthermore, IR spectra of adsorbed pyridine indicate that the nanosized sulfated zirconia contains relatively more Brønsted acidic sites than conventional sulfated zirconia. Catalytic tests show that the nanosized sulfated zirconia exhibits much higher activity than conventional sulfated zirconia in catalytic esterification of cyclohexanol with acetic acid.

1. Introduction

Zirconia used as a catalyst or catalytic support has been paid much attention recently.[1−8] Generally, the surface area of zirconia is relatively low. To increase the surface area of zirconia, various methods, including preparation of nanocrystalline,[2−5] mesostructured[6,7] and meso−macroporous zirconia,[8] have been used. Among the family of zirconia, sulfated zirconia is potentially important for industrial reactions such as hydrocarbon isomerization, alkylation, and esterification.[9−17] However, the relatively small surface area of sulfated zirconia strongly limits its wide application in catalytic reactions. Therefore, sulfated zirconia with a large surface area has always been sought.

There have been a number of successful examples of the preparation of sulfated zirconia that has relatively large surface area.[18−30] For example, sulfated zirconia has been supported into the pores of ordered mesostructured silica,[18−23] mesoporous sulfated zirconia has been synthesized from various surfactants,[24−27] sulfated zirconia nanopaticles have been prepared by reverse microemulsion and a sol−gel technique,[28] and both monoclinic and tetragonal sulfated zirconia with high surface area have been prepared by a one-step crystallization method.[29,30] Notably, the preparative process of these materials is relatively complicated, and solvents must be used.

It is well-known that many factors can influence acidity of sulfated zirconia catalysts, such as preparation procedure, crystalline phase of zirconia, calcination temperature, sulfur species, surface area, and water content.[31−36] As for preparation procedure, the type of precursor for preparing sulfated zirconia plays a vital role in the final texture and in the performance of the catalyst. Generally, amorphous $Zr(OH)_4$ must be used as the precursor for sulfation. Sulfation of crystallized zirconium oxide cannot produce strong acidity.[12] Moreover, calcination temperature is another important factor for the catalytic activity of the catalyst. The most common calcination temperature for sulfated zirconia ranges from 550 to 650 °C.

The nature of active sites on the sulfated zirconia has been investigated extensively, and it is generally accepted that sulfated zirconia contains both Brønsted and Lewis acidic sites, but there is still arguing that the strong acid sites in sulfated zirconia result from Lewis,[37,38] Brønsted,[39,40] or a combination of both acid sites.[41,42] For example, in *n*-butane isomeration, it has been agreed that *n*-butene might be formed by dehydrogenation of *n*-butane at first.[43,44] However, researchers proposed various routes for the formation of *n*-butene, including Brønsted acidic sites[45,46] or Lewis acidic sites[47,48] or both types of acidic sites[49,50] on sulfated zirconia catalysts.

Here we present a simple route for preparation of nanosized sulfated zirconia with a large surface area (165−193 m^2/g) from calcination of $ZrOCl_2 \cdot 8H_2O$ mixed with $(NH_4)_2SO_4$ at 600 °C in the absence of any solvent. IR spectra of adsorbed pyridine indicate that the nanosized sulfated zirconia contains more Brønsted acidic sites. Catalytic data show that the nanosized sulfated zirconia exhibits higher activity than conventional sulfated zirconia in esterification of cyclohexanol with acetic acid that is a typical reaction catalyzed by Brønsted acidic sites.

2. Experimental Section

2.1. Preparation of Samples. Typical procedures for preparing nanosized sulfated zirconia, designated as S-ZrO_2, were as follows: (1) $ZrOCl_2 \cdot 8H_2O$ and $(NH_4)_2SO_4$ with a molar ratio of 1:6 were ground in a carnelian mortar for 20 min at room temperature, and (2) after placement for 18 h at room temperature, the sample was calcined for 5 h at 600 °C.

* Corresponding author. Fax: +86-(431)-5168590. E-mail: fsxiao@mail.jlu.edu.cn.
[†] Jilin University.
[‡] Chinese Academy of Sciences.

10.1021/jp046335a CCC: $30.25
Published on Web 01/22/2005

For comparison, conventional sulfated zirconia, designated as SZ, was prepared by the calcination of $Zr(OH)_4$ precursor impregnated with 0.5 M $(NH_4)_2SO_4$ solution at temperature of 600 °C for 3 h. $ZrOCl_2 \cdot 8H_2O$ calcined at 600 °C for 5 h is designated as ZrO_2-c; $Zr(SO_4)_2 \cdot 4H_2O$ calcined at 600 °C for 5 h is designated as ZrO_2-s.

2.2. Characterization of Samples. X-ray diffraction (XRD) patterns were obtained with a Siemens D5005 diffractometer using Cu Kα radiation ($\lambda = 1.5405$ Å). The crystalline size of tetragonal phase was determined from the characteristic peak ($2\theta = 30.4°$ for the (111) reflection) using Scherrer's equation: $D = K\lambda/\beta \cos\theta$, where $K = 0.9$, D represents crystallite size, λ represents the wavelength of Cu Kα radiation, and β represents the corrected half-width of the diffraction peak. Infrared (IR) spectra of the samples as well as the spectra of pyridine adsorbed on the samples were recorded on a Nicolet FT-IR spectrometer (Impact 410) with a resolution of 1 cm^{-1}. Before measurement of pyridine adsorption, the samples were pressed to thin wafers (10 mg/cm^2) and placed into a quartz cell equipped with CaF_2 windows. The sample disks were evacuated at 400 °C for 2 h (10^{-5} Torr) and cooled to room temperature. Then 10 Torr of pyridine was exposed to the disks at room temperature. After the adsorption at room temperature for 1 h and evacuation at 300 °C for 1 h, the infrared spectra were recorded. Transmission electron microscopy (TEM) images and electron diffraction (ED) patterns were recorded on a JEOL 2010 with an acceleration voltage of 200 kV. The nitrogen isotherms at 77 K were measured using a Micromeritics ASAP 2010 system. The pore-size distribution for mesopores was calculated using the Barrett−Joyner−Halenda (BJH) model. Thermogravimetric and differential thermal analysis (TG-DTA) were carried out on a NETZSCH STA 449C with a heating rate of 20 K/min from room temperature to 1000 °C. The sample was mounted horizontally and purged with a synthetic airflow of 100 mL/min.

2.3. Catalytic Reactions. Cumene and 1,3,5-triisopropylbenzene (TIPB) cracking reactions were performed at 300 °C by pulse injections. In each run, 50 mg of catalyst was used, 0.4 μL reactant was injected by pulse, and nitrogen was used as the carrier gas at a flow rate of 53.7 mL/min. The reaction products were analyzed by a Shimadzu GC-8A equipped with a TCD detector.

Catalytic esterification of cyclohexanol with acetic acid was performed in a 100 mL flask. The flask was kept in a constant-temperature bath with a temperature control of ±1 °C, and the reaction mixture was magnetically stirred. A thermowell with a thermometer was used to monitor the temperature. During the experiment, acetic acid was always in stoichiometric excess over the reactant alcohol. As a typical run, the catalyst was first introduced into the reactor and brought to the reaction temperature, while the reactor contents were stirred. Then, the alcohol was added into the reactor at the same temperature as the reaction mixture and the moment of addition of alcohol was taken as the starting time of the reaction. Samples were withdrawn from the reactor at regular intervals, quenched, and analyzed by gas chromatography (Shimadzu GC-17A) with a FID detector. A capillary column packed with 5% OV-17 was used for quantitative analysis of the reaction products.

The isomerization of *n*-butane to isobutane was carried out in a fixed-bed continuous flow reactor under atmospheric pressure. First 0.35 g of the catalyst was loaded into the reactor and then pretreated in flowing dry air (20 mL/min) at 450 °C for 3 h, followed by a decrease of the temperature to 250 °C.

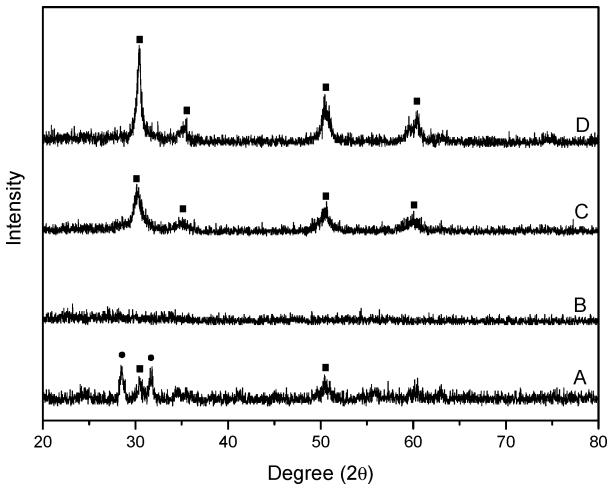

Figure 1. XRD patterns of ZrO_2-c (A), ZrO_2-s (B), S-ZrO_2 (C), and SZ (D); (■) tetragonal phase of zirconia and (●) monoclinic phase of zirconia.

The feed consisted of a mixture of 2 mL/min of *n*-butane and 20 mL/min of H_2. The weight hourly space velocity (WHSV) is 0.89 g of *n*-butane per gram catalyst per hour. An on-line gas chromatograph equipped with FID was used to analyze the reaction products.

3. Results

3.1. X-ray Diffraction (XRD). Figure 1 shows XRD patterns of ZrO_2-c, ZrO_2-s, S-ZrO_2, and SZ samples. Obviously, the XRD pattern of ZrO_2-c prepared by calcination of $ZrOCl_2 \cdot 8H_2O$ shows peaks assigned to both tetragonal phase and monoclinic phase of zirconia. ZrO_2-s does not exhibit any peak, suggesting the amorphous nature of zirconia. In contrast, the XRD pattern of S-ZrO_2 exhibits only peaks characteristic of the tetragonal phase of zirconia. This indicates that $(NH_4)_2SO_4$ is very important for the restraint of the monoclinic phase of zirconia. Comparatively, conventional SZ also shows peaks characteristically assigned to the tetragonal phase of zirconia, but the width of the peaks are much narrower than that of the peaks in S-ZrO_2. This suggests that zirconia particles in S-ZrO_2 are much smaller than those in SZ. By Scherrer's equation, the average size of tetragonal zirconia crystallines in S-ZrO_2 is estimated to be 7 nm.

3.2. Transmission Electron Microscopy (TEM). Figure 2 shows TEM images of S-ZrO_2. Generally, ZrO_2 particles in S-ZrO_2 have been aggregated each other, forming mesopores with the size of about 6 nm (Figure 2A). However, after ultrasonic dispersion for 10 min, we can observe clearly that ZrO_2 particles in S-ZrO_2 are nanocrystallines, their size mainly being 5−9 nm (Figure 2B), in good agreement with the crystallite size estimated by XRD (Figure 1). Moreover, when we enlarged the image of incompletely dispersed S-ZrO_2 sample, it can be shown more clearly that the S-ZrO_2 sample contains mesopores whose size is about 6 nm aggregated by the nanocrystallines (Figure 2C).

3.3. N_2 Adsorption−Desorption Isotherms. Figure 3 shows N_2 adsorption−desorption isotherms of S-ZrO_2. A hysteresis loop at high relative pressure is observed, which is generally due to the capillary condensation associated with mesopores. Correspondingly, BJH pore size distribution for S-ZrO_2 is narrow and gives a mean value at 6.3 nm (inset). Possibly, the mesoporosity may be assigned to the aggregation of nanoparticles with each other. Interestingly, a high BET surface area

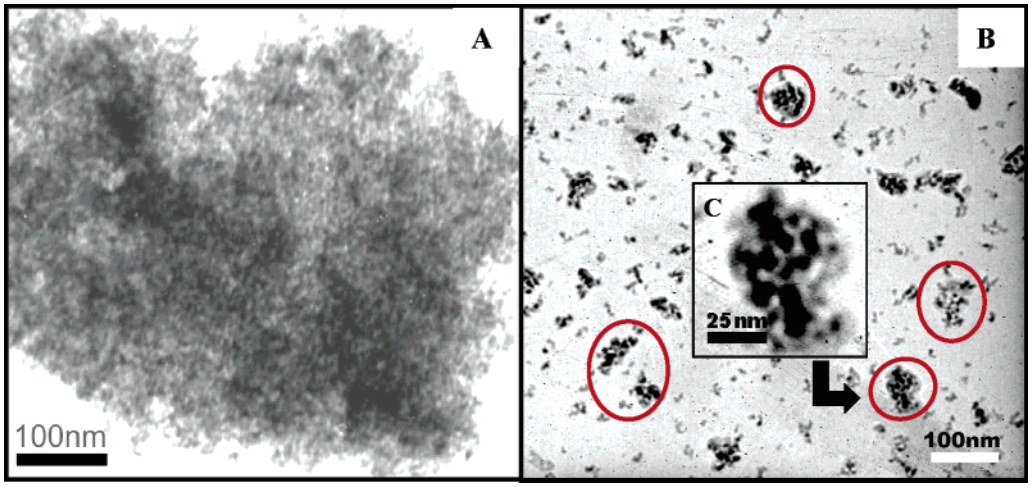

Figure 2. TEM images of S-ZrO_2: (A) the image before ultrasonic dispersion, (B) the image after ultrasonic dispersion, and (C) the magnified image of the selected area.

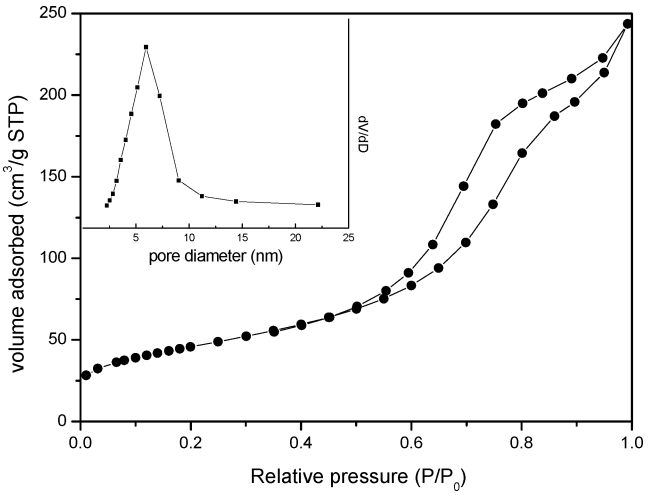

Figure 3. N_2 adsorption/desorption isotherm and pore distribution plots (inset) of S-ZrO_2 (when the ratio of $(NH_4)_2SO_4/ZrOCl_2 \cdot 8H_2O$ is 6:1).

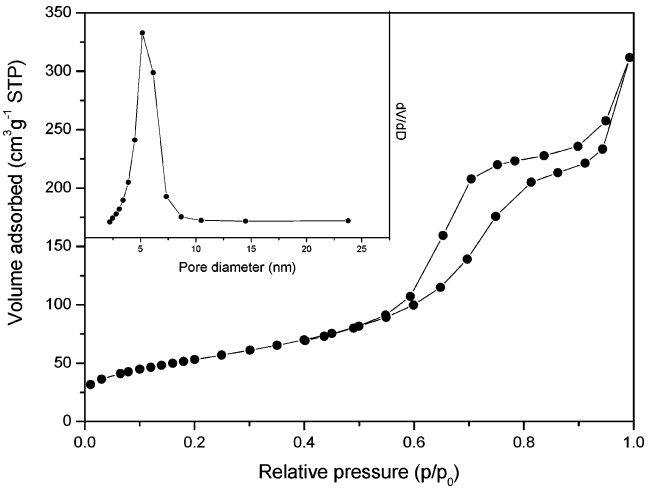

Figure 4. N_2 adsorption/desorption isotherm and pore distribution plots (inset) of S-ZrO_2 (when the ratio of $(NH_4)_2SO_4/ZrOCl_2 \cdot 8H_2O$ is 10:1).

of 165.1 m^2/g and a large pore volume of 0.34 cm^3/g are observed for S-ZrO_2. Furthermore, when the molar ratio of $(NH_4)_2SO_4/ZrOCl_2 \cdot 8H_2O$ is 10:1, the sample of S-ZrO_2 exhibits higher BET surface area (193 m^2/g) and more uniform pore distribution (Figure 4). In contrast, the adsorption data of SZ (Figure S1 in Supporting Information) exhibit a relatively low

TABLE 1: Textural Properties and Catalytic Activities of Various Samples

samples	calcination temp (°C)	BET surf. area (m^2/g)	pore vol (cm^3/g)	sulfate content (%)	% conversion cumene[a]	% conversion TIPB[a]
ZrO_2-c	600	33.4	0.04	0	<5	<5
ZrO_2-s	600	49	0.05	32.4	41.6	59.3
SZ	600	86.8	0.10	4.3	76.3	88.1
S-ZrO_2	600	165.1	0.34	7.7	80.4	100

[a] Cumene and 1,3,5-triisopropylbenzene (TIPB) cracking reactions were performed at 300 °C by pulse injections. In each run, 50 mg of catalyst was used, 0.4 μL reactant was injected by pulse, and nitrogen was used as the carrier gas at a flow rate of 53.7 mL/min.

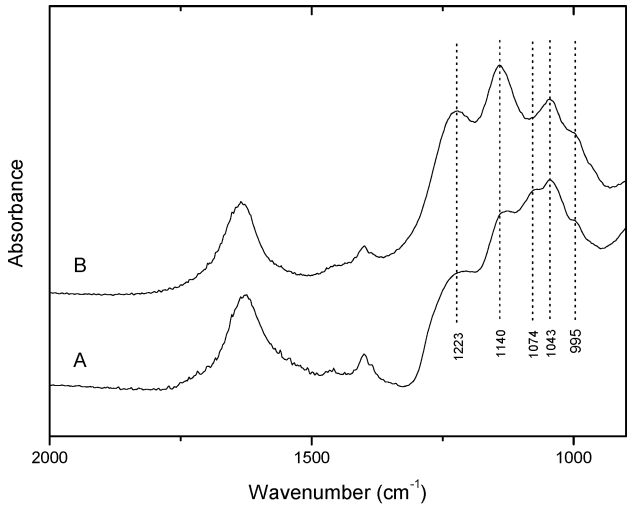

Figure 5. IR spectra of SZ (A) and S-ZrO_2 (B).

BET surface area (86.8 m^2/g, Table 1) and pore volume (0.10 cm^3/g, Table 1). These results indicate that our preparative method for S-ZrO_2 is unique.

3.4. Infrared (IR) Spectroscopy. Figure 5 shows IR spectra of various samples. S-ZrO_2 exhibits obvious bands at 995, 1043, 1140, 1223 cm^{-1} assigned to typical bands for chelating bidentate sulfate ion coordinated to zirconium cation.[24,51] Comparatively, conventional SZ shows an additional band at 1074 cm^{-1}, except for the bands in S-ZrO_2. These results suggest that sulfur species in the two samples may be a little different. Furthermore, IR spectra of adsorbed pyridine (Figure 6) show that both samples contain Lewis (1450 cm^{-1}) and Brønsted

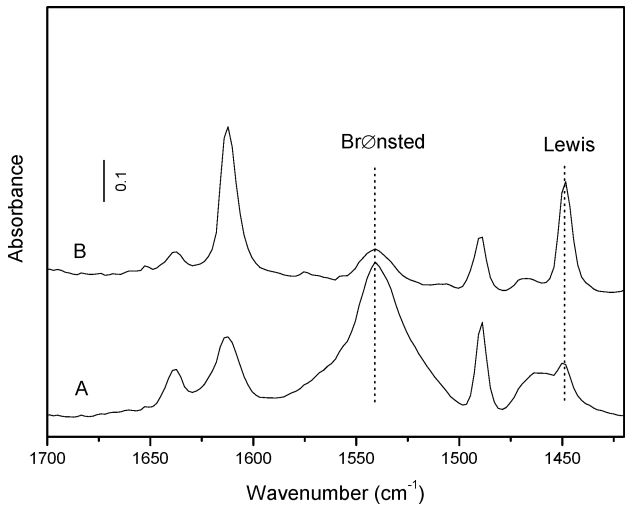

Figure 6. IR spectra of pyridine adsorbed on S-ZrO_2 (A) and SZ (B).

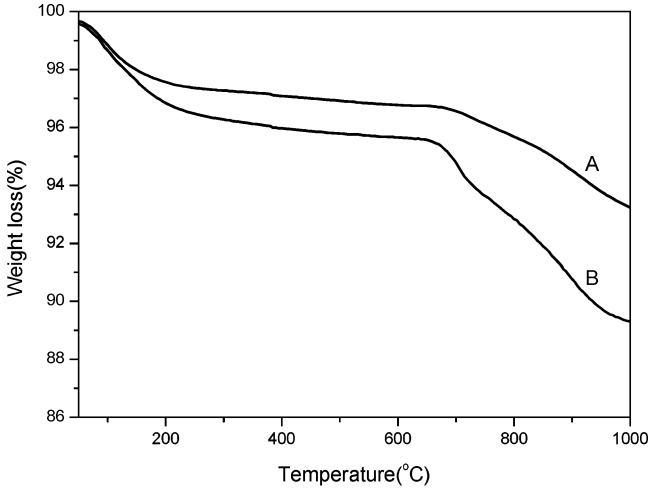

Figure 7. TG curves of SZ (A) and S-ZrO_2 (B).

acidic sites (1540 cm^{-1}).[52] However, the integral area on the 1540 cm^{-1} band for S-ZrO_2 is much larger than that for SZ, indicating that S-ZrO_2 contains much more Brønsted acidic sites than SZ. This might be related to the difference in the sulfur species on the surface of S-ZrO_2 and SZ (Figure 5).

3.5. Thermogravimetric (TG) Analysis. Figure 7 shows the TG curves of SZ and S-ZrO_2. Both samples exhibit two weight losses at 25−400 and 600−1000 °C, which are assigned to the removal of water and decomposition of sulfate, respectively. However, it is interesting to note that the weight loss of S-ZrO_2 sample is larger than that of SZ. In the region of 600−1000 °C, the weight loss of S-ZrO_2 and SZ is at 7.7% and 4.3%, respectively, indicating that S-ZrO_2 contains more sulfur species than SZ. Possibly, S-ZrO_2 contains more acidic sites than SZ.[12]

3.6. Catalytic Activity. It is well-known that cracking reactions of cumene and 1,3,5-triisopropylbenzene are typical acidic catalytic reactions. Table 1 presents catalytic activities in cracking of cumene and 1,3,5-triisopropylbenzene of various samples. Obviously, ZrO_2-c is almost inactive (<5%) and SZ is really active (76.3% in cumene cracking and 88.1% in TIPB cracking, respectively). Notably, S-ZrO_2 shows higher activities (80.4% in cumene cracking and 100% in TIPB cracking) than ZrO_2-c, ZrO_2-s, and SZ, which indicates that S-ZrO_2 is a better acidic catalyst.

Esterification is a typical reaction catalyzed by Brønsted acidic sites, and esterification of cyclohexanol with acetic acid

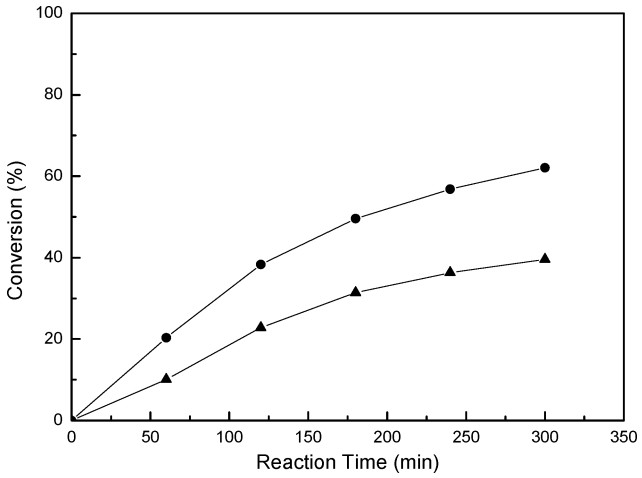

Figure 8. Dependence of cyclohexanol conversion on reaction time over SZ (▲) and S-ZrO_2 (●) catalysts. The esterification of cyclohexanol with acetic acid was carried out with a mole ratio of cyclohexanol/acetic acid of 1:3, temperature at 100 °C, and catalyst loading of 5% (w/w) based on alcohol.

is useful in industrial purposes, such as synthesis of flavors.[53] Figure 8 shows the dependence of activity on reaction time in esterification of cyclohexanol with acetic acid. Notably, S-ZrO_2 exhibits much higher catalytic activity than SZ during the reaction. For example, when the reaction time reaches 300 min, conventional SZ gives 40% conversion of cyclohexanol, while S-ZrO_2 exhibits 62% conversion. These results confirm that S-ZrO_2 contains more Brønsted acidic sites than conventional SZ.

For deep comparison, catalytic activities for S-ZrO_2 and conventional SZ were also tested on *n*-butane isomerization (Figure S2 in Supporting Information). As similar to previous reports, conventional SZ is active (18% at 5 min) for the conversion of *n*-butane to isobutane. However, S-ZrO_2 exhibits very low conversion (4.2% at 5 min). Possibly, the lower activity for *n*-butane isomerization over S-ZrO_2 than that over conventional SZ should be directly attributed to different sulfur species and acidic sites in the two samples.

3.7. Al-Promoted S-ZrO_2. It has been reported that Al-promoted sulfated zirconia shows higher catalytic activity and better stability than nonpromoted sulfated zirconia.[54,55] Similarly, Al-promoted S-ZrO_2 is successfully prepared by the simple calcination of $(NH_4)_2SO_4$, $ZrOCl_2 \cdot 8H_2O$, and $Al_2(SO_4)_3 \cdot 18H_2O$. When the ratio of $(NH_4)_2SO_4/ZrOCl_2 \cdot 8H_2O$ is 6:1 and aluminum amount is 3 mol % as Al_2O_3, Al-promoted S-ZrO_2 exhibits a surface area of 195 m^2/g, which is much higher than that (165 m^2/g) of S-ZrO_2 with the same molar ratio of $(NH_4)_2SO_4/ZrOCl_2 \cdot 8H_2O$. The sample of Al-promoted S-ZrO_2 gives typical IV isotherms and uniform pore distribution (Figure S3 in Supporting Information). Obviously, the simple calcination is a general route for preparation of sulfated zirconia with various promoters.

4. Discussion

4.1. Preparative Method. It is well-known that the preparation for conventional sulfated zirconia generally involves hydrolyzation of zirconium source, drying of zirconium hydroxide, sulfation, activation of the sulfated sample, and calcination of the sample.[13] Obviously, the preparative process is complex. In contrast, the preparation of S-ZrO_2 is relatively simple in the present work, which is only a simple calcination of mixed $(NH_4)_2SO_4$ and $ZrOCl_2 \cdot 8H_2O$. More importantly, it

is solvent-free for the preparation of S-ZrO_2. On the contrary, solvent is necessary for the preparation of conventional sulfated zirconia.[13] Obviously, solvent-free preparation of S-ZrO_2 is an environmental benign method,[56] compared with the preparation of conventional sulfated zirconia.

4.2. Surface Area. Because catalysis is a surface phenomenon, generally catalysts having larger surface area will have higher catalytic activity. Interestingly, when the molar ratio of $(NH_4)_2SO_4/ZrOCl_2\cdot 8H_2O$ is 6:1, S-ZrO_2 prepared by a simple calcination shows very high surface area (165 m^2/g, Table 1), compared with that of conventional sulfated zirconia (87 m^2/g, Table 1). Furthermore, when the molar ratio of $(NH_4)_2SO_4/ZrOCl_2\cdot 8H_2O$ is 10:1, the sample of S-ZrO_2 exhibits much higher surface area, giving a BET surface area of 193 m^2/g. When the ratio of $(NH_4)_2SO_4/ZrOCl_2\cdot 8H_2O$ is 6:1 and the aluminum amount is 3 mol % as Al_2O_3, Al-promoted S-ZrO_2 exhibits a BET surface area of 195 m^2/g. All of these results confirm that S-ZrO_2 prepared by a simple calcination in the absence of solvent has much larger BET surface area than conventional sulfated zirconia.

4.3. Phase, Sulfur Species, and Acidic Sites in Sulfated Zirconia. Generally, it is believed that the presence of the tetragonal phase in sulfated zirconia is an important factor for the formation of acidic sites. In our case, S-ZrO_2 shows a pure phase assigned to tetragonal crystalline of zirconia, which is consistent with that of conventional sulfated zirconia. This result suggests that S-ZrO_2 shows the possibility for the formation of acidic sites. Moreover, the presence of sulfur species is another important factor for the formation of acidic sites in sulfated zirconia. It has been reported that the sulfur species on sulfated zirconia is very complex.[13,14] Notably, as observed in IR spectra (Figure 5), the sulfur species on S-ZrO_2 is a little different than that on SZ. Furthermore, TG results (Figure 7) show that S-ZrO_2 contains more sulfur species than SZ. The difference in sulfur species between S-ZrO_2 and conventional sulfated zirconia may be related to the difference in their acidic sites. As shown in Figure 6, IR spectra of adsorbed pyridine show that S-ZrO_2 has much more Brønsted acidic sites than SZ, and catalytic tests of cracking and esterification show that S-ZrO_2 has higher activities than conventional sulfated zirconia (Figure 8, Table 1).

4.4. Proposed Mechanism for Formation of Nanosized Sulfated Zirconia (S-ZrO_2). As observed in Figure 2, the size of zirconia in sulfated zirconia (S-ZrO_2) is very uniform and nanoscaled (5−9 nm), which is reasonably assigned to our unique preparative method. It is worthy to note that $(NH_4)_2SO_4$ is excessive during calcination of $(NH_4)_2SO_4$ mixed with $ZrOCl_2\cdot 8H_2O$ for the preparation of nanosized sulfated zirconia. Possibly, excessive $(NH_4)_2SO_4$ interacts with zirconium species sufficiently, retarding the growth of the zirconia particles. This hypothesis is further supported by the preparation of S-ZrO_2 with higher molar ratio of $(NH_4)_2SO_4/ZrOCl_2\cdot 8H_2O$. For example, when the molar ratio of $(NH_4)_2SO_4/ZrOCl_2\cdot 8H_2O$ is 10:1, the sample of S-ZrO_2 exhibits a higher surface area of 193 m^2/g (Figure 4) and a smaller particle size of near 4−6 nm.

5. Conclusions

Nanosized sulfated zirconia with a large surface area (165−193 m^2/g) and Brønsted acidic sites has been successfully prepared from a simple calcination in the absence of any solvent. The results of XRD and TEM show that S-ZrO_2 is nanosized crystallines. N_2 adsorption of S-ZrO_2 exhibits typical IV isotherms, which are similar to those of mesoporous materials. Combined with the results of TEM, it is revealed that the mesoporosity in S-ZrO_2 is aggregated by nanoparticles. Characterization of the sample by IR indicates that S-ZrO_2 contains more Brønsted acidic sites. Various catalytic reactions including cracking of cumene and 1,3,5-triisopropylbenzene, esterification of cyclohexanol with acetic acid, and *n*-butane isomerization are used for evaluating the catalyst. The esterification confirms that S-ZrO_2 contains more Brønsted acidic sites than conventional sulfated zirconia.

Acknowledgment. This work was supported by National Natural Science Foundation of China, BASF, CNPC, Ministry of Education of China, State Basic Research Project of China, and National Advanced Materials Committee of China (2002AA321010).

Supporting Information Available: N_2 adsorption/desorption isotherm of SZ, dependence of *n*-butane conversion on reaction time over SZ and S-ZrO_2 catalysts, and N_2 adsorption/desorption isotherm and pore distribution of Al-promoted S-ZrO_2. The material is available free of charge via the Internet at http://pubs.acs.org.

References and Notes

(1) Tanabe, K. *Mater. Chem. Phys.* **1985**, *13*, 347; Yamaguchi, T. *Catal. Today* **1994**, *20*, 199.
(2) Chuah, G. K.; Jaenicke, S.; Cheong, S. A.; Chan, K. S. *Appl. Catal. A* **1996**, *145*, 267.
(3) Wu, N. L.; Wang, S. Y.; Rusakova, I. A. *Science* **1999**, *285*, 1375.
(4) Joo, J.; Yu, T.; Kim, Y. W.; Park, H. M.; Wu, F.; Zhang, J. Z.; Hyeon, T. *J. Am. Chem. Soc.* **2003**, *125*, 6553.
(5) Xu, B.-Q.; Wei, J.-M.; Yu, Y.-T.; Li, Y.; Li, J.-L.; Zhu, Q.-M. *J. Phys. Chem. B* **2003**, *107*, 5203.
(6) Knowles, J. A.; Hudson, M. J. *Chem. Commun.* **1995**, 2083; *J. Mater. Chem.* **1996**, *6*, 89.
(7) Yang, P.; Zhao, D.; Margolese, D. I.; Chmelka, B. F.; Stucky, G. D. *Nature* **1998**, *396*, 612; *Chem. Mater.* **1999**, 2813.
(8) Blin, J.-L.; Leonard, A.; Yuan, Z.-Y.; Gigot, L.; Vantomme, A.; Cheetham, A. K.; Su, B.-L. *Angew. Chem., Int. Ed.* **2003**, *42*, 2872.
(9) Hino, M.; Arata, K. *Chem. Commun.* **1980**, 851.
(10) Davis, B. H.; Keogh, R. A.; Srinivasan, R. *Catal. Today* **1994**, *20*, 219.
(11) Clearfield, A.; Serrette, G. P. D.; Khazi-Syed, A. H. *Catal. Today* **1994**, *20*, 295.
(12) Corma, A. *Chem. Rev.* **1995**, *95*, 559.
(13) Song, X. M.; Sayari, A. *Catal. Rev. Sci. Eng.* **1996**, *38*, 320.
(14) Yadav, G. D.; Kirthivasan, N. *Chem. Commun.* **1995**, 203; Yadav, G. D.; Nair, J. J. *Microporous Mesoporous Mater.* **1999**, *33*, 1.
(15) Hsu, C. Y.; Heimbuch, C. R.; Armes, C. T.; Gates, B. C. *J. Chem. Soc., Chem. Commun.* **1992**, 1645; Cheung, T.-K.; d'Itri, J. L.; Gates, B. C. *J. Catal.* **1995**, *151*, 464; Cheung, T.-K.; Gates, B. C. *Top. Catal.* **1998**, *6*, 41.
(16) Xu, B.-Q.; Sachtler, W. M. H. *J. Catal.* **1997**, *167*, 224.
(17) Sommer, J.; Jost, R.; Hachoumy, M. *Catal. Today* **1997**, *38*, 309.
(18) Chen, C. L.; Cheng, S.; Lin, H. P.; Wong, S. T.; Mou, C. Y. *Appl. Catal. A* **2001**, *215*, 21; Chen, C. L.; Li, T.; Cheng, S.; Lin, H. P.; Bhongale, C. J.; Mou, C. Y. *Micropor. Mesopor. Mater.* **2001**, *50*, 201.
(19) Xia, Q.-H.; Hidajat, K.; Kawi, S. *Chem. Commun.* **2000**, 2229; Xia, Q.-H.; Hidajat, K.; Kawi, S. *J. Catal.* **2002**, *205*, 318.
(20) Sun, Y. Y.; Zhu, L.; Lu, H.; Wang, R.; Lin, S.; Jiang, D.; Xiao, F.-S. *Appl. Catal. A* **2002**, *237*, 21.
(21) Matsuhashi, H.; Tanaka, M.; Nakamura, H.; Arata, K. *Appl. Catal. A* **2001**, *208*, 1.
(22) Hua, W. M.; Tang, Y.; Yue, Y. H.; Gao, Z. *J. Mol. Catal. A* **2001**, *170*, 195.
(23) Landau, M. V.; Titelman, V.; Vradman, L.; Wilson, P. *Chem. Commun.* **2003**, 594.
(24) Huang, Y. Y.; McCarthy, T. J.; Sachlter, W. M. H. *Appl. Catal. A: Gen.* **1996**, *148*, 135.
(25) McIntosh, A. J.; Kydd, R. A. *Microporous Mesoporous Mater.* **2001**, *37*, 281.
(26) Yang, X.; Jentoft, F. C.; Jentoft, R. E.; Girgsdies, F.; Ressler, T. *Catal. Lett.* **2002**, *81*, 25.
(27) Sun, Y. Y.; Yuan, L. N.; Wang, W.; Chen, C. L.; Xiao, F.-S. *Catal. Lett.* **2003**, *86*, 57; Sun, Y. Y.; Yuan, L. N.; Ma, S. Q.; Han, Y.; Zhao, L.; Wang, W.; Chen, C. L.; Xiao, F.-S. *Appl. Catal. A: Gen.* **2004**, *268*, 17.

(28) Althues, H.; Kasel, S. *Langmuir* **2002**, *18*, 7428; Mishra, M. K.; Tyagi, B.; Jasra, R. V. *Ind. Eng. Chem. Res.* **2003**, *42*, 5727.
(29) Stichert, W.; Schuth, F. *J. Catal.* **1998**, *174*, 242.
(30) Stichert, W.; Schuth, F.; Kuba, S.; Knozinger, H. *J. Catal.* **2001**, *198*, 277.
(31) Tanabe, K.; Hattori, H.; Yamaguchi, T. *Crit. Rev. Surf. Chem.* **1990**, *1*, 1.
(32) Chen, F. R.; Courdurier, G.; Joly, J.; Vedrine, J. C. *J. Catal.* **1993**, *143*, 616.
(33) Babou, F.; Bigot, B.; Sauset, P. *J. Phys. Chem.* **1993**, *97*, 11501.
(34) Morterra, C.; Cerrato, G.; Bolis, V. *Catal. Today* **1993**, *17*, 505.
(35) Corma, A.; Juan-Rajadell, A. I.; Lopez Nieto, J. M. *Appl. Catal. A* **1994**, *116*, 151.
(36) Gonzalez, M. R.; Kobe, J.; Fogash, K. B.; Dumesic, J. A. *J. Catal.* **1996**, *160*, 290; Kobe, J. M.; Gonzalez, M. R.; Fogash, K. B.; Dumesic, J. A. *J. Catal.* **1996**, *164*, 459.
(37) Bensitel, M.; Saur, O.; Lavalley, J.-C. *Mater. Chem. Phys.* **1987**, *17*, 249.
(38) Pinna, F.; Signoretto, M.; Strukul, G.; Cerrato, G.; Morterra, C. *Catal. Lett.* **1994**, *26*, 339.
(39) Scrinivasan, R.; Keogh, R. A.; Davis, B. H. *Catal. Lett.* **1996**, *36*, 51.
(40) Babou, F.; Bigot, B.; Sautet, P. *J. Phys. Chem.* **1993**, *97*, 11501.
(41) Katada, N.; Endo, J.; Notsu, K.; Yasunobu, N.; Naito, N.; Niwa, M. *J. Phys. Chem. B* **2000**, *104*, 10321.
(42) Davis, B. H.; Keogh, R. A.; Srinivasan, R. *Catal. Today* **1994**, *20*, 219.
(43) Farcasiu, D.; Ghenciu, A.; Li, J. Q. *J. Catal.* **1996**, *158*, 116.
(44) Ghenciu, A.; Farcasu, D. *Catal. Lett.* **1997**, *44*, 29.
(45) Tran, M.-T.; Gnep, N. S.; Szabo, G.; Guisnet, M. *Appl. Catal. A* **1998**, *171*, 207.
(46) Adeeva, V.; Liu, H.; Xu, B.; Sachtler, W. M. H. *Top. Catal.* **1998**, *6*, 61.
(47) Corma, A.; Fornes, V.; Juan-Rajadell, M. I.; Lopez Nieto, J. M. *Appl. Catal. A* **1994**, *116*, 151.
(48) Zhang, C.; Miranda, R.; Davis, B. H. *Catal. Lett.* **1994**, *29*, 349.
(49) Pinna, F.; Signoretto, M.; Strukul, G.; Cerrato, G.; Morterra, C. *Catal. Lett.* **1994**, *26*, 339.
(50) Chen, F. R.; Coudurier, G.; Joly, J.; Vedrine, J. C. *J. Catal.* **1993**, *143*, 616.
(51) Babou, F.; Coudurier, G.; Vedrine, J. C. *J. Catal.* **1995**, *152*, 341.
(52) Davis, B. H.; Keogh, R. A.; Alerasool, S.; Zalewski, D. J.; Day, D. E.; Doolin, P. K. *J. Catal.* **1999**, *183*, 45.
(53) Yadav, G. D.; Mehta, P. H. *Ind. Eng. Chem. Res.* **1994**, *33*, 2198.
(54) Xia, Y. D.; Hua, W. M.; Tang, Y.; Gao, Z. *Chem. Commun.* **1999**, 1899; Hua, W. M.; Xia, Y. D.; Yue, Y. H.; Gao, Z. *J. Catal.* **2000**, *196*, 104.
(55) Hua, W.; Sommer, J. *Appl. Catal. A* **2002**, *227*, 279.
(56) Raja, R.; Sankar, G.; Thomas, J. M. *J. Am. Chem. Soc.* **2001**, *123*, 8153.